Global and regional axial ocean angular momentum signals and length-of-day variations (1985–1996)

Rui M. Ponte
Atmospheric and Environmental Research, Inc., Cambridge, Massachusetts

Detlef Stammer
Physical Oceanography Research Division, Scripps Institution of Oceanography, La Jolla, California

Abstract

Changes in ocean angular momentum about the polar axis (M) are related to fluctuations in zonal currents (relative component M_r) and latitudinal shifts in mass (planetary component M_Ω). Output from a 1° ocean model is used to calculate global M_r, M_Ω, and M time series at 5-day intervals for the period January 1985–April 1996. The annual cycle in M_r, M_Ω, and M is larger than the semiannual cycle, and M_Ω amplitudes are nearly twice those of M_r. Year-to-year modulation of the seasonal cycle is present, but interannual variability is weak. The spectrum of M is red (background slope between ω^{-1} and ω^{-2}) at subseasonal periods, implying a white or blue spectrum for the external torque on the ocean. Comparisons with previous studies indicate the importance of direct atmospheric forcing in inducing subseasonal M signals, relative to instabilities and other internal sources of rapid oceanic signals. Regional angular momentum estimates show that seasonal variability tends to be larger at low latitudes but there are many local maxima due to the spatial structure of zonal current and mass variability. At seasonal timescales, latitudes ~20°S–10°N contribute substantial variability to M_Ω, while signals in M_r can be traced to Antarctic Circumpolar Current transports and associated circulation. Variability in M is found to be small when compared with similar time series for the atmosphere and the solid Earth, but ocean signals are significantly coherent with atmosphere-solid Earth residuals, implying a measurable oceanic impact on length-of-day variations.

1. Introduction

As a rotating geophysical fluid, the oceans possess angular momentum M about the polar axis consisting of a planetary component M_Ω, due to the solid body rotation, and a relative component M_r, due to their zonal circulation. Study of the axial ocean angular momentum (OAM) is important to the understanding of the variable Earth's rotation. In the absence of external torques, the planet conserves its angular momentum. Thus changes in OAM or in atmospheric angular momentum (AAM) should be mirrored in records of the length-of-day (LOD). The close link between AAM and LOD at seasonal and shorter timescales has long been established, but loss of coherence appears at periods of about a month and amplitudes drop below significant levels at subweekly periods (see reviews by *Hyde and Dickey* [1991] and *Rosen* [1993] and papers therein). The ocean is thus expected to contribute at the residual level at seasonal timescales and become more important at higher frequencies.

Knowledge of the oceanic mass and zonal velocity fields and their variability is required to assess OAM and its role in closing the planet's angular momentum budget. Partly because of the lack of data, the first OAM studies focused only on relative component associated with individual currents such as the Antarctic Circumpolar Current (ACC) [*Munk and MacDonald*, 1960; also *Ponte and Rosen*, 1994, hereafter PR94, and references therein]. Modeling developments over the last decade, however, have produced a number of simulations of the global ocean circulation and thus provided a new tool to estimate axial OAM [e.g., *Brosche et al.*, 1990; PR94; *Bryan*, 1997, hereafter B97; *Ponte*, 1997; *Segschneider and Sündermann*, 1997; *Johnson et al.*, 1999]. *Marcus et al.* [1998] have demonstrated the measurable impact of OAM signals on LOD fluctuations at timescales from 1 year to 10 days. Other studies [*Ponte*, 1990; *Holloway and Rhines*, 1991; *Straub*, 1993; *Cummins*, 1995] have also used the angular momentum framework to examine aspects of the ocean circulation related to the role of stress and pressure torques at the atmosphere and solid Earth interfaces.

Despite the recent revived interest in the subject, knowledge of OAM continues to be sketchy and primarily focused on the seasonal variability of M_r. Most of what is known comes from simple (forward) model simulations without any data constraints and is inherently uncertain, although the comparisons with AAM and LOD are encouraging [PR94; *Marcus et al.*, 1998]. Calculations of M_r from simulated zonal currents depend on the model friction parameterizations, bottom topography representation, and surface forcing, as has been noted by B97 (e.g., available estimates of annual cycle in M_r vary by a factor of two). Calculations of M_Ω, based on values of bottom pressure diagnosed from model density and sea level fields, are considerably more uncertain because of unrealistic density trends present in most models and because of the impact of the Boussinesq approximation (and in some models the rigid lid assumption) on the sea level fields [PR94; B97; *Ponte*, 1999]. New modeling studies are thus expected to provide further insight on M_r and M_Ω signals and their uncertainties.

Here we use output from a run of the newly developed model of *Marshall et al.* [1997] to extend previous studies of axial OAM. *Ponte et al.* [1998] and *Ponte and Stammer* [1999] have used the same output to demonstrate the role of the equatorial components of OAM in the excitation of polar motion, at the same time attesting for the quality of the model fields. After describing model and data sets in section 2, global OAM quantities are treated in section 3, together with comparisons with previous results from other models that allow further insight into the uncertainties of model-based OAM estimates. Section 4 discusses regional OAM quantities and their relation to global values, in particular those related to M_Ω whose regional characteristics are for the first time revealed here. The impact of OAM signals on LOD, discussed first by *Marcus et al.* [1998] using a different model, is revisited in section 5 and for a much longer period. A summary and some general remarks conclude the paper.

2. OAM and Ancillary Datasets

Our definitions and calculation of OAM quantities follow closely PR94 and *Ponte et al.* [1998]. A fluid particle of density ρ and unit volume, rotating about the Earth's polar axis, has axial angular momentum m given by

$$m = m_\Omega + m_r = \rho\Omega r^2 \cos^2\phi + \rho r \cos\phi\, u \quad (1)$$

where r and Ω are the mean Earth radius and rotation rate, respectively, ϕ denotes latitude, u is zonal velocity relative to solid body rotation, and m_Ω and m_r are the planetary and relative components of the particle's angular momentum. Integrating (1) over the ocean volume and using the hydrostatic relation

$p_z = -g\rho$, with p being pressure and g being the acceleration of gravity, yields for the total planetary and relative OAM components

$$M_\Omega = \frac{\Omega r^4}{g} \int\int p_b \cos^3\phi \; d\phi \; d\lambda = \frac{C\Omega}{0.7}\chi_3^P \qquad (2)$$

$$M_r = \frac{r^3}{g} \int\int\int u \cos^2\phi \; d\phi \; d\lambda \; dp = C\Omega\chi_3^V \qquad (3)$$

Here λ is longitude, p_b is the pressure at the ocean bottom, and we have set the surface pressure to zero. The variables χ_3^P and χ_3^V are, respectively, the pressure and velocity excitation functions derived by *Barnes et al.* [1983] and commonly used in computing the effects of the geophysical fluids on LOD. χ_3^P and χ_3^V are basically equivalent to M_Ω and M_r but nondimensionalized by $C\Omega$, where $C = 7.04 \times 10^{37}$ kg m^2 is the polar moment of inertia of the mantle. The extra factor of 0.7 in χ_3^P accounts for the effects of solid Earth deformation under loading. Thus, only 70% of the M_Ω signals are effectively involved in LOD excitation. We will use χ values when analyzing OAM in the context of the planet's momentum budget and M_r, M_Ω values otherwise, but conversion between the two quantities is straightforward using (2) and (3).

Model output used to calculate M_Ω and M_r is the same as in *Ponte et al.* [1998] and *Ponte and Stammer* [1999]. For these studies, the model of *Marshall et al.* [1997] was run on a near-global domain (80°S–80°N) with 1°x1° horizontal grid spacing and 20 vertical levels. Step-like topography was used. The model was started from the final state of a 3-year spin-up run and forced with twice-daily surface wind stresses and daily surface heat and freshwater fluxes from the National Centers for Environmental Prediction, in addition to surface restoring to climatological temperature and salinity fields. More details on the model output can be found in the papers cited above and also *Stammer et al.* [1997]. Integrals in (2) and (3) are carried over the model ocean domain, with p_b values estimated as in *Ponte* [1999]. The spatially-uniform sea level correction of *Greatbatch* [1994] was applied to account for global ocean volume changes due to unmodeled steric effects. With this correction, the total oceanic mass in the model is constant in time.

To study the role of OAM signals on the planet's angular momentum budget, values of AAM or χ^A based on the National Centers for Environmental Prediction/National Center for Atmospheric Research reanalysis, are obtained from the Sub-Bureau for Atmosphere of the International Earth Rotation Service. Estimates of both χ^V and χ^P are used. Contributions from winds up to 10 hPa levels are included in χ^V; values of χ^P are based on the inverted barometer assumption [*Salstein et al.*, 1993], consistent with the timescales analyzed here [*Ponte*, 1997]. Geodetic excitation functions χ^G are computed from SPACE97 LOD time series [e.g., *Gross*, 1996].

All angular momentum and χ series are calculated for more than 11 years (January 1985–April 1996) and are provided as 5-day averages. Besides globally-integrated OAM time series, we also calculate regional integrals over boxes of 1° x 1° (the horizontal resolution of the model), which will be denoted as $\hat{M}_\Omega$, $\hat{M}_r$. The sum of gridded values over all boxes yields the respective globally-integrated values. However, local integrals are based only on monthly-averaged quantities and thus capture mostly the seasonal variability. The gridded $\hat{M}_\Omega$, $\hat{M}_r$ values are used to assess the importance of different basins and regions in contributing to the seasonal cycle in OAM. No torque or momentum flux terms are available from this run, however, and no attempt is made to examine the OAM budget, either regionally or globally.

3. Global OAM Variability

Time series of M_Ω, M_r, and their sum M in Figure 1 display variability at seasonal and shorter timescales, with weak interannual signals and no apparent secular trends. The annual cycle is clear in all time series, but with visible year-to-year amplitude modulations (e.g. M strong in 1989, weak in 1994). Signals in M_Ω tend to be larger than those in M_r and noticeably so at the annual period. The importance of M_Ω is consistent with Ekman and geostrophic dynamics that imply the ocean mainly adjusts to seasonally varying stress and pressure torques by changing its planetary angular momentum [PR94]. The relative importance of M_Ω is in stark contrast with what happens in the atmosphere, where M_r dominates seasonal variability [e.g., *Salstein et al.*, 1993] and nonlinear eddy processes are important [*Peixoto and Oort*, 1992]. The M_r and M_Ω terms in Figure 1 are positively correlated, with a coefficient of 0.69. Because of the positive correlation, variability in M is larger than that in either M_Ω or M_r, with peak-to-peak amplitudes $\sim 10^{25}$ kg m^{2}s^{-1} or $\sim$10% of the range of variability in AAM [e.g., *Rosen*, 1993]. The correlation between M_r and M_Ω is expected for geostrophic dynamics, in which zonal currents are related to meridional pressure gradients and thus to latitudinal distri-

bution of mass.

Spectra of M_Ω, M_r, and M in Figure 2 show that power in M_Ω is larger than that in M_r over all frequencies (but less so as frequency increases), contributing most of the power in M. Nevertheless, all spectra exhibit similar shapes and a background slope between ω^{-1} and ω^{-2}. Such frequency dependence for spectrum of M implies a white or blue spectrum for the net external torque acting on the ocean, which is a sum of the surface zonal wind stress torque and east-west pressure and stress torques on the bottom boundary [*Ponte*, 1990; B97]. As the spectrum of the surface stress torque on the oceans is predominantly red (not shown), ocean dynamics play a fundamental role in determining the character of OAM variability resulting from atmospheric forcing.

For a qualitative measure of the low frequency variability, the periodograms of M_Ω, M_r, and M are also shown in Figure 2. There is a tendency for whiteness at interannual timescales with a peak at the annual period. The overall importance of M_Ω in explaining changes in M at all frequencies is clear. Despite the short records and the year-to-year modulation noted in Figure 1, we perform a harmonic analysis on 11 complete years of data (1985–95) to characterize annual and semiannual cycles. Respective amplitudes and phases are given in Table 1. Amplitudes of M_Ω are nearly double those of M_r, for both annual and semiannual periods, but nearly in phase (particularly for the former). Annual cycle is almost twice as large as the semiannual cycle. Relative phasing of the annual and semiannual cycles leads to a clear maximum in OAM values in the late boreal summer (Figure 1).

The present estimate of the annual cycle in M_r has an amplitude of about half that of PR94, with a maximum occurring approximately 1 month later, but is much more similar, both in amplitude and phase, to those reported by B97 for most of his experiments, except the one with smooth topography, and also with those in *Brosche et al.* [1990]. For the semiannual cycle, amplitude spread is much wider, with values in Table 1 being about 2 to 3 times larger than those of B97 and PR94, and 7 times larger than those in *Brosche et al.* [1990]. With the exception of PR94, semiannual maximum occurs always in late February to late March (and 6 months later). Overall, M_r phase estimates seem to be more stably determined than amplitudes.

Plausible reasons for the range in seasonal M_r values include differences in forcing fields (e.g., PR94 and B97 use climatological monthly mean winds), eddy parameterizations and resolution (e.g., PR94 estimates are based on 0.5° x 0.5° grid, with better resolved eddies), and bottom topography. The degree of smoothness of the topography field was found by B97 to have the largest influence on the annual cycle of M_r, compared to changes in wind fields and viscosity parameters. *Marcus et al.* [1998] also speculate on the role of topography representation in improving OAM estimates. We note that our model has comparable vertical resolution (20 levels) to that of PR94, but uses less smooth topography. The comparison with B97 values is thus consistent with the idea that rougher, more realistic topography may yield smaller annual amplitudes in M_r.

A comparison of present and previous M_Ω (and thus M) estimates is not as straightforward, because of the different assumptions made in dealing with the seasonal steric sea level component. We restrict discussion to values of B97, who uses the same method to correct for unmodeled steric effects. Compared to B97 values computed with ECMWF wind climatology for 1986–92 (see his Table 4), amplitudes in Table 1 are similar but somewhat larger for both the annual and semiannual cycles, and annual maximum occurs 1 month later and semiannual maxima occur a couple of weeks earlier. Note that the different upper surface formulations in the two models (rigid lid in B97, free surface in our case) appears to have a relatively small impact on the calculation of M_Ω.

Besides differences at the seasonal time scale, the subseasonal OAM variability in PR94 is much weaker than that shown in Figure 1. Time series of PR94 are based on an eddy-resolving model forced by monthly mean winds. The differences with the non-eddy resolving, synoptically-forced estimates in Figure 1 thus suggest that intrinsic oceanic instabilities and related eddies are not as important as atmospherically-driven variability in producing rapid OAM signals, and that knowledge of wind stresses is essential in studies of such OAM signals (*Ponte* [1997] makes the case for the importance of surface pressure at subweekly periods). This finding contrasts with the apparent dominant contribution of intrinsic eddy processes to surface variability in many oceanic regions [e.g., *Stammer*, 1998]. Globally-integrated OAM of course favors barotropic signals coherent on the largest scales, and these may be essentially atmospherically-driven. But eddies generated by oceanic instabilities may also carry little net angular momentum signals (either implying weak interaction with or nearly compensat-

ing torques on the bottom boundary). More definite answers to these issues must await calculations with fully-resolved eddies (eddy field in the model used by PR94 is only marginally resolved and its strength underestimated).

4. Regional OAM Seasonal Variability

An analysis of regional OAM variability can shed light on the importance of given circulation features to global OAM. The importance of u and p_b signals involved in $\hat{M}_r$ and $\hat{M}_\Omega$, respectively, increases with proximity to the equator where the moment arm $a\cos\phi$ is largest, but variability in u and p_b also differs substantially from region to region (see Figure 8b in *Ponte and Stammer* [1999]) due to differences in ocean dynamics, forcing, bathymetry, etc. Our discussion of regional OAM signals at seasonal timescale complements analysis of $\hat{M}_r$ signals by PR94 and provides a first description of $\hat{M}_\Omega$ signals, setting the stage also for future studies of regional OAM budgets, when local torques and flux terms will be available. We consider local integrals over 10° x 10° boxes to focus on the large scale.

Figure 3a shows the standard deviation of $\hat{M}_r$, and the fractional covariance, defined as

$$\frac{\langle(\hat{M}_r - \langle\hat{M}_r\rangle)(M_r - \langle M_r\rangle)\rangle}{\langle(M_r - \langle M_r\rangle)^2\rangle}$$

where angular brackets represent time averaging, is shown in Figure 3b to highlight relation between local and global quantities. By its definition, fractional covariances over all grid boxes sum up to unity. Variability in $\hat{M}_r$ is strongest in the tropics, particularly in the Pacific and Indian oceans, where zonal circulation is known to have a strong seasonal modulation, and consistent with results in PR94 and B97. Much of the tropical variability, and more generally the basin variability, is, however, expected to recirculate at different latitudes, as oceanic flows are to zeroth order horizontally nondivergent. The recirculation can be inferred from the alternating bands of negative and positive fractional covariances, strikingly aligned in the zonal direction especially in the Pacific, Indian, and Southern oceans.

Major contributions to seasonal variability in M_r are likely to come from the Southern Ocean where unblocked zonal flow through Drake Passage is possible. The positive covariances at ~60°–20°S latitudes add up to nearly one and indicate the importance of including flows up to subtropical southern latitudes to capture full seasonal variability in M_r (similar to finding by PR94). Knowing the ACC transport T through the Drake Passage, and assuming perfectly nondivergent flow, one can estimate M_r as $2\pi r^2\rho\,\overline{\cos^2\phi}\,T$ [*Munk and MacDonald*, 1960; PR94], where $\overline{\cos^2\phi}$ is based on some representative latitude. Figure 4 shows such an estimate in comparison to the globally integrated M_r. The similarity between the two curves is clear at the seasonal timescale. (At shorter time scales, the assumption of horizontally nondivergent flows becomes less valid, but analysis not shown reveals significant coherence between Drake Passage transport and M_r at all frequencies. The correlation coefficient between the two series is 0.66.)

Variability in $\hat{M}_\Omega$, examined in Figure 5a, is weaker and not as spatially variant as that in $\hat{M}_r$. As before, the Pacific and Indian Oceans show larger signals than the Atlantic. Despite a tendency for weaker variability at high latitudes, there are local maxima in the Southern Ocean (west of South America and southwest of Australia) and in the western North Pacific. These regions were first noted for their large subseasonal p_b fluctuations [*Fukumori et al.*, 1998], but show similar enhancement at seasonal periods [*Ponte*, 1999; *Ponte and Stammer*, 1999]. Spatial variability of the wind stress curl or topographic features leading to a much reduced effective β may yield a locally enhanced response [*Ponte*, 1999]. Variability in coastal, shallow seas (e.g., Sea of Japan, South China Sea, Arafura Sea between Australia and New Guinea) can be surprisingly large. These constricted regions are not optimally resolved in the model, but results seem to agree with the output of other models run at much higher resolution (cf. Plate 1 in *Ponte* [1999]). Large p_b (and thus $\hat{M}_\Omega$) signals in shallow areas can be expected given that wind stress forcing terms scale inversely with ocean depth. The large variability in equatorial regions may also be related to the strong monsoonal forcing, as well as the different dynamics of the equatorial wave guide.

The relation between $\hat{M}_\Omega$ and M_Ω is quite different than for M_r. With few exceptions, mainly at high latitudes, positive covariances dominate in Figure 5b, indicating adding contributions to M_Ω over most regions. Covariances are, however, small (maximum below 0.02) in comparison with the case of M_r in Figure 3b. The contributions from the Atlantic are weakest compared to the other oceans. Tropical latitudes (~20°S–10°N) contribute most strongly to seasonal M_Ω signals. The characteristics of $\hat{M}_\Omega$ reflect the weak but very large scale nature of seasonal anomalies

in p_b [*Ponte*, 1999].

With $\hat{M}_r$ signals being stronger than those in $\hat{M}_\Omega$, the pattern of variability in $\hat{M}$ (Figure 6a) follows in general that of $\hat{M}_r$, with maxima in tropical Indian and Pacific Oceans. These maxima coincide with maximum positive covariances in Figure 6b. Comparing Figures 3b, 5b, and 6b, $\hat{M}$ has a weaker banded structure than seen in Figure 3b because of the positive contributions over most regions from $\hat{M}_\Omega$. Thus the structure of added covariances in longitude in Figure 6b resembles that in Figure 3b, but values are generally positive and most important in two bands at ~20°–40°S and ~10°–20°N. In the Southern Ocean, $\hat{M}_\Omega$ variability compensates somewhat for that in $\hat{M}_r$ and decreases the importance of the latter at ~40°–50°S.

5. OAM, AAM and LOD

The impact of OAM signals in Figure 1 on the planet's axial angular momentum budget is assessed by comparing them to observed AAM and LOD variability. The motivation for this analysis is to check the degree to which our OAM estimates represent measurable signals in LOD. Attempting a "best" angular momentum budget would involve thorough analysis of all the time series involved, including AAM and LOD, and is beyond our intended scope.

Figure 7 compares the oceanic χ_3^O, atmospheric χ_3^A, and geodetic χ_3^G time series, and spectra and coherence results are displayed in Figure 8. (Note that, in calculating χ_3^O, effects of M_Ω are reduced by 30%; see discussion in section 2.) As noted in the Introduction, time series of χ_3^G and χ_3^A are closely linked and almost indistinguishable to the eye. Variability in residuals $\chi_3^G - \chi_3^A$ (or χ_3^{G-A} for short) is at around 10% of that in either series, and most conspicuous at subseasonal periods. Spectra of χ_3^G and χ_3^A have very similar shapes and power levels at all periods resolved, consistent with a dominant relation between AAM and LOD. Power levels in χ_3^G are, however, generally higher, indicating missing LOD excitation. (Largest discrepancies occur near the fortnightly band, where χ_3^G spectrum shows some enhancement not matched by χ_3^A spectrum; incomplete removal of solid Earth tide in the χ_3^G series may be responsible for this feature.)

Figures 7 and 8 clearly show the weak variability in χ_3^O compared to χ_3^G or χ_3^A. Variance in χ_3^O is only 6% of that in χ_3^A, and also small (31%) compared to that in the residual χ_3^{G-A}. Spectrum of χ_3^O shows weaker power than that in χ_3^{G-A} spectrum at all frequency bands. Variability in OAM is, however, significantly coherent with the residual series χ_3^{G-A} at most periods (Figure 8), demonstrating the presence of correlated signals in both series. Furthermore, adding OAM to AAM signals increases the coherence with LOD in general and most clearly at periods of 13–18 days, providing also for slight improvements in the phase estimates (i.e., values closer to zero).

Our results agree qualitatively with the findings of *Marcus et al.* [1998] and confirm the observable role of OAM signals in the planet's axial angular momentum budget. However, the amount of atmosphere-solid Earth residual variance explained by our estimated OAM signals is small (only 10%) compared to their best results (42% in the case of the Miami Isopycnal Coordinate Ocean Model run). Besides the different ocean models and periods analyzed, there are also two important differences in the way AAM series are computed. First, *Marcus et al.* AAM values include wind contributions from the uppermost levels of the atmosphere (10–0.3 hPa), which seem to reduce substantially the seasonal χ_3^{G-A} residuals and may effectively improve agreement with OAM signals at seasonal period. Second, *Marcus et al.* do not consider M_Ω contributions to AAM. We find that by similarly neglecting atmospheric M_Ω signals, χ_3^{G-A} variance explained by OAM signals rises to ~20%. However, in this case, variance in χ_3^{G-A} also goes up by more than 30% and high frequency coherence between χ_3^G and χ_3^A is generally lower than in Figure 8. (In fact, residual rms magnitude in Figure 7 is smaller than that reported by *Marcus et al.* (52.7 μs vs. 60.5 μs using LOD units), and coherence amplitudes in Figure 8 are noticeably higher compared to their Figure 3b. Thus, it seems that including M_Ω signals in AAM provides better agreement with LOD.) For these reasons, conclusions regarding the relative value of the different OAM series would be premature.

6. Summary and Final Remarks

We have examined more than 11 years of axial OAM signals calculated from output of a 1° model. Seasonal and shorter period signals are clear in both M_r and M_Ω, but signals in M_Ω are generally stronger. Interannual variability is weak. There is a clear annual cycle, with amplitude nearly twice that of the semiannual cycle, and modulation from year to year. Atmospheric driving is found important for the presence of subseasonal OAM signals. Strength of sea-

sonal signals varies considerably with region. Low latitudes contribute substantially to fluctuations in M_Ω, but there are other important signals over the Southern Ocean and other regions. The ACC and related circulation in Southern Ocean are closely related to M_r; strong $\hat{M}_r$ signals are also present at low latitudes but they are associated with recirculating currents at different latitudes and largely cancel out. OAM signals can explain some of the observed changes in LOD but their estimated amplitudes are substantially smaller than atmosphere-solid Earth residuals.

It is interesting to note the similarity in the relation between regional and global M_r signals (banded structure in Figure 3b), and regional and global zonal wind stress torques (cf. Figure 5 in *Ponte and Rosen* [1993]). Previous works have shown the in-phase relation between seasonal signals in total M_r and stress torque [PR94; B97]. Thus, both regionally and globally, M_r and wind torques vary nearly in phase. This behavior is rather surprising, since for angular momentum balance a driving torque should lead OAM by 90°. Results of *Ponte* [1990] and B97 point to a plausible explanation. Seasonal wind stress and pressure torques nearly balance instantaneously, but the pressure torque lags slightly given the finite (albeit rapid) adjustment time in the oceans. Consequently, as can be easily seen by drawing a phasor diagram, the small resulting net torque should lead the wind torque by nearly 90°. (B97 noted this peculiar phase relation but left it unexplained.) Viscous torques further reduce the amplitude of this net torque but do not affect its phase (see Figure 12 of B97). From the relation between wind and net torques and from angular momentum conservation, it follows that M_r and wind torque should be in phase as observed. The arguments have been presented for global quantities but should essentially hold regionally too [PR94].

From the comparisons between present and previous results, it is clear that ocean models will give different axial OAM time series, depending on their formulations, forcing, bathymetry, etc. Using axial OAM series in the context of the planet's angular momentum budget may provide a useful global consistency check on the models, much as proposed in the context of polar motion [*Ponte et al.*, 1998]. Comparisons in a more controlled setting, as carried out, for example, by *Hide et al.* [1997] for the atmosphere, should be most useful in this regard.

Both *Marcus et al.* [1998] and our results give weak OAM signals compared to the atmosphere-solid Earth residuals, at all frequency bands examined; similar findings are discussed by *Ponte* [1997] and *Johnson et al.* [1999]. It remains to be determined whether this behavior is due to underestimating the strength of OAM contributions (χ_3^O and χ_3^{G-A} spectra are similar in shape and models are known to underestimate oceanic variability), to errors in χ_3^G and χ_3^A (note the dropping with frequency of coherence amplitudes between χ_3^G and χ_3^A and the comparable power in χ_3^A and χ_3^{G-A} series at fortnightly and shorter periods), or to missing excitation sources not related to atmosphere or oceans. A more detailed examination of the axial angular momentum budget exploring all these issues is left for future work. In what regards improving OAM estimates and assessing their uncertainties, an important next step currently being pursued involves the use of state estimation methods to constrain the model to data.

Acknowledgments. D. Spiegel (MIT) helped with the numerical computations. P. Nelson (AER) helped with data sets, analysis of model output, and figures. We thank F. Bryan for his comments. R.P. is supported by the NASA Solid Earth and Natural Hazards program (contracts NAS5-97270 and NAS5-98182). D.S. is supported by JPL contract 958125 and NASA grants NAG5-7162 and NAG5-3724.

References

Barnes, R. T. H., R. Hide, A. A. White, and C. A. Wilson, Atmospheric angular momentum fluctuations, length-of-day changes and polar motion. *Proc. R. Soc. London, Ser. A, 387*, 31–73, 1983.

Brosche, P., J. Wünsch, A. Frische, J. Sündermann, E. Maier-Reimer, and U. Mikolajewicz, The seasonal variation of the angular momentum of the oceans, *Naturwissenschaften, 77*, 185–186, 1990.

Bryan, F. O., The axial angular momentum balance of a global ocean general circulation model, *Dyn. Atmos. Oceans, 25*, 191–216, 1997.

Cummins, P., Relative angular momentum balances of quasi-geostrophic circulation models, *J. Mar. Res., 53*, 315–340, 1995.

Fukumori, I., R. Raghunath, and L.-L. Fu, Nature of global large-scale sea level variability in relation to atmospheric forcing: A modeling study, *J. Geophys. Res., 103*, 5493–5512, 1998.

Greatbatch, R. J., A note on the representation of steric sea level in models that conserve volume rather than mass, *J. Geophys. Res., 99*, 12,767–12,771, 1994.

Gross, R. S., Combinations of Earth orientation measurements: SPACE94, COMB94, AND POLE94. *J. Geophys. Res., 101*, 8729–8740, 1996.

Hide, R., and J. O. Dickey, Earth's variable rotation, *Science, 253*, 629–637, 1991.

Hide, R., J. O. Dickey, S. L. Marcus, R. D. Rosen, and D. A. Salstein, Atmospheric angular momentum fluctuations during 1979–1988 simulated by global circulation models, *J. Geophys. Res., 102*, 16,423–16,438, 1997.

Holloway, G., and P. Rhines, Angular momenta of modeled ocean gyres, *J. Geophys. Res., 96*, 843–846, 1991.

Johnson, T. J., C. R. Wilson, and B. F. Chao, Oceanic angular momentum variability estimated from the parallel ocean climate model, 1988-1993, *J. Geophys. Res., 104*, 25,183–25,195, 1999.

Marcus, S. L., Y. Chao, J. O. Dickey, and P. Gegout, Detection and modeling of nontidal oceanic effects on Earth's rotation rate, *Science, 281*, 1656–1659, 1998.

Marshall, J., A. Adcroft, C. Hill, L. Perelman, and C. Heisey, A finite-volume, incompressible Navier Stokes model for studies of ocean on parallel computers, *J. Geophys. Res., 102*, 5753–5766, 1997.

Munk, W.H., and G.J.F. MacDonald, *The Rotation of the Earth*. Cambridge University Press, 323 pp, 1960.

Peixoto, J.P., and A.H. Oort, *Physics of Climate*, American Institute of Physics, New York, 520 pp, 1992.

Ponte, R. M., Barotropic motions and the exchange of angular momentum between the oceans and solid earth, *J. Geophys. Res., 95*, 11369–11374, 1990.

Ponte, R. M., Oceanic excitation of daily to seasonal signals in Earth rotation: results from a constant-density numerical model, *Geophys. J. Int., 130*, 469–474, 1997.

Ponte, R. M., A preliminary model study of the large-scale seasonal cycle in bottom pressure over the global ocean, *J. Geophys. Res., 104*, 1289–1300, 1999.

Ponte, R. M., and R. D. Rosen, Determining torques over the ocean and their role in the planetary momentum budget, *J. Geophys. Res., 98*, 7317–7325, 1993.

Ponte, R. M., and R. D. Rosen, Oceanic angular momentum and torques in a general circulation model, *J. Phys. Oceanogr., 24*, 1966–1977, 1994.

Ponte, R. M., and D. Stammer, Role of ocean currents and bottom pressure variability on seasonal polar motion, *J. Geophys. Res., 104*, 23,393–23,409, 1999.

Ponte, R. M., D. Stammer, and J. Marshall, Oceanic signals in observed motions of the Earth's pole of rotation, *Nature, 391*, 476–479, 1998.

Rosen, R. D., The axial momentum balance of Earth and its fluid envelope, *Surv. Geophys., 14*, 1–29, 1993.

Salstein, D. A., D. M. Kann, A. J. Miller, and R. D. Rosen, The sub-bureau for atmospheric angular momentum of the international earth rotation service: a meteorological data center with geodetic applications, *Bull. Amer. Meteor. Soc., 74*, 67–80, 1993.

Segschneider, J., and J. Sündermann, Response of a global ocean circulation model to real-time forcing and implications to Earth's rotation, *J. Phys. Oceanogr., 27*, 2370–2380, 1997.

Stammer, D., On eddy characteristics, eddy transports, and mean flow properties, *J. Phys. Oceanogr.*, 28, 727–739, 1998.

Stammer, D., C. Wunsch, R. Giering, Q. Zhang, J. Marotzke, J. Marshall, and C.N. Hill, The global ocean circulation estimated from TOPEX/POSEIDON altimetry and the MIT general circulation model. *MIT Center of Global Change Science, Report 49*, 1997.

Straub, D., On the transport and angular momentum balance of channel models of the Antarctic Circumpolar Current. *J. Phys. Oceanogr., 23*, 776–782, 1993.

R. M. Ponte, Atmospheric and Environmental Research, Inc., 840 Memorial Drive, Cambridge, MA 02139 USA. (ponte@aer.com)

D. Stammer, Physical Oceanography Research Division, Scripps Institution of Oceanography, 8605 La Jolla Shores Dr., La Jolla, CA 92093-0230. (dstammer@ucsd.edu)

–; revised –; accepted –.

This preprint was prepared with AGU's LaTeX macros v4. File rpaper formatted April 4, 2000.

Figure 1. Time series of M_Ω, M_r, and M. For ease of comparison between curves, time means have been removed.

Figure 2. Spectra and low-frequency periodograms of M_Ω (dotted lines), M_r (dashed lines), and M (solid lines). Spectra are based on averaging over 20 adjacent frequency bands. First spectral point represents the 414–138 day band. Before Fourier transformation, series are tapered at both ends with a half-cosine bell.

Figure 3a. Standard deviation of $\hat{M}_r$ in kg m^{2}s^{-1}. Contour interval is 10^{22} kg m^{2}s^{-1}.

Figure 3b. Fractional covariance of $\hat{M}_r$ with M_r. Contour interval is 0.01. Light shading denotes negative values. Right panel shows fractional covariances added over longitude.

Figure 4. Variability in ACC transport at Drake Passage calculated in OAM units as described in the text for $\phi = 55°$ (solid line) and the globally integrated value of M_r (dotted line). Small gaps in ACC transport series have been linearly interpolated.

Figure 5a. As in Figure 3a but for $\hat{M}_\Omega$.

Figure 5b. As in Figure 3b but for $\hat{M}_\Omega$. Contour interval is 2×10^{-3}.

Figure 6a. As in Figure 3a but for $\hat{M}$.

Figure 6b. As in Figure 3b but for $\hat{M}$. Contour interval is 2.5×10^{-3}.

Figure 7. Time series of χ_3^G, χ_3^A, and χ_3^O (solid lines). Dotted line in bottom panel is the residual χ_3^{G-A}. Note the difference in scale. All time series have been detrended and high-pass filtered to supress variability at periods of 3.8 years and longer.

Figure 8. (a) Spectra of χ_3^G (dotted-dashed line), χ_3^A (dashed line), χ_3^{G-A} (solid line) and χ_3^O (dotted line) calculated as in Figure 2. (b) Coherence amplitude squared between χ_3^G and $\chi_3^A+\chi_3^O$ (solid line), χ_3^G and χ_3^A (dashed line), and χ_3^{G-A} and χ_3^O (dotted line). Values above 0.15 are significantly different than zero at 95% confidence level. (c) Respective coherence phases in degrees.

Table 1. Amplitude in 10^{23}kg m^2 s^{-1} and Phase (Date of the First Maximum After January 1) of M_Ω, M_r, and M for the Annual and Semiannual Periods.

	Annual		Semiannual	
	Amp	Phase	Amp	Phase
M_Ω	7.8	Aug 27	4.4	Mar 15
M_r	3.6	Sept 1	2.1	Feb 24
M	11.4	Aug 28	6.2	Mar 9

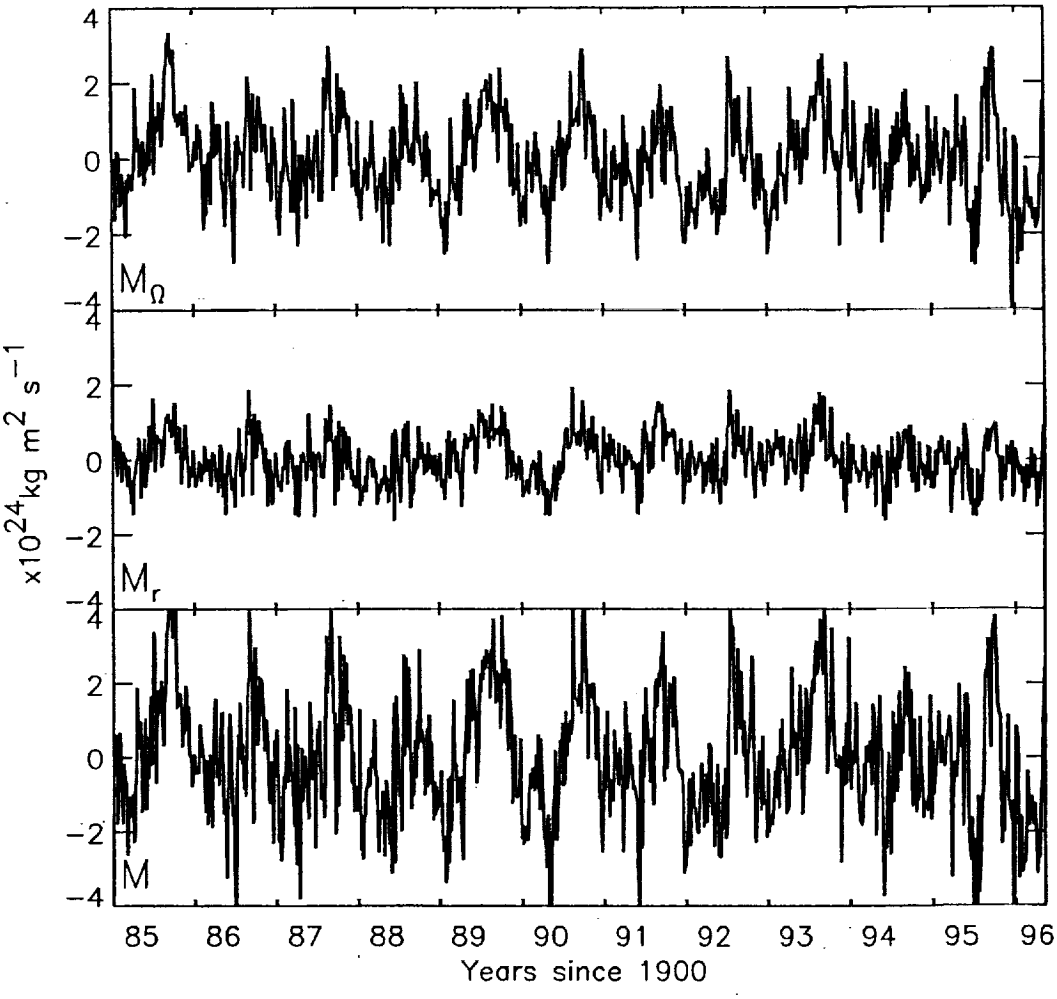
4
2
0
−2
−4
M_Ω
M_r
M
$x10^{24}$kg m^2 s^{-1}
85
86
87
88
89
90
91
92
93
94
95
96
Years since 1900

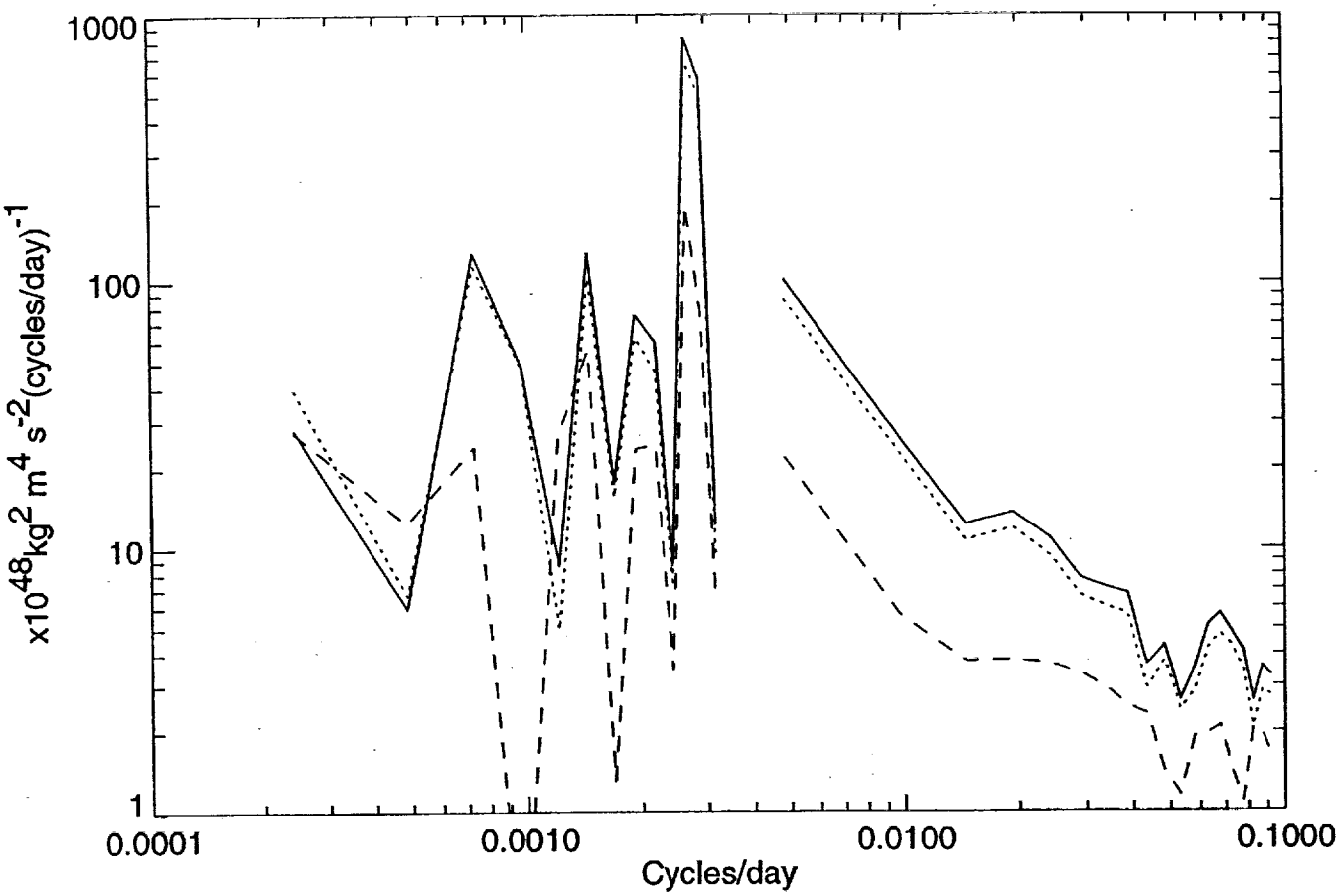
1000
100
10
1
x10^48 kg^2 m^4 s^-2 (cycles/day)^-1
0.0001
0.0010
0.0100
0.1000
Cycles/day

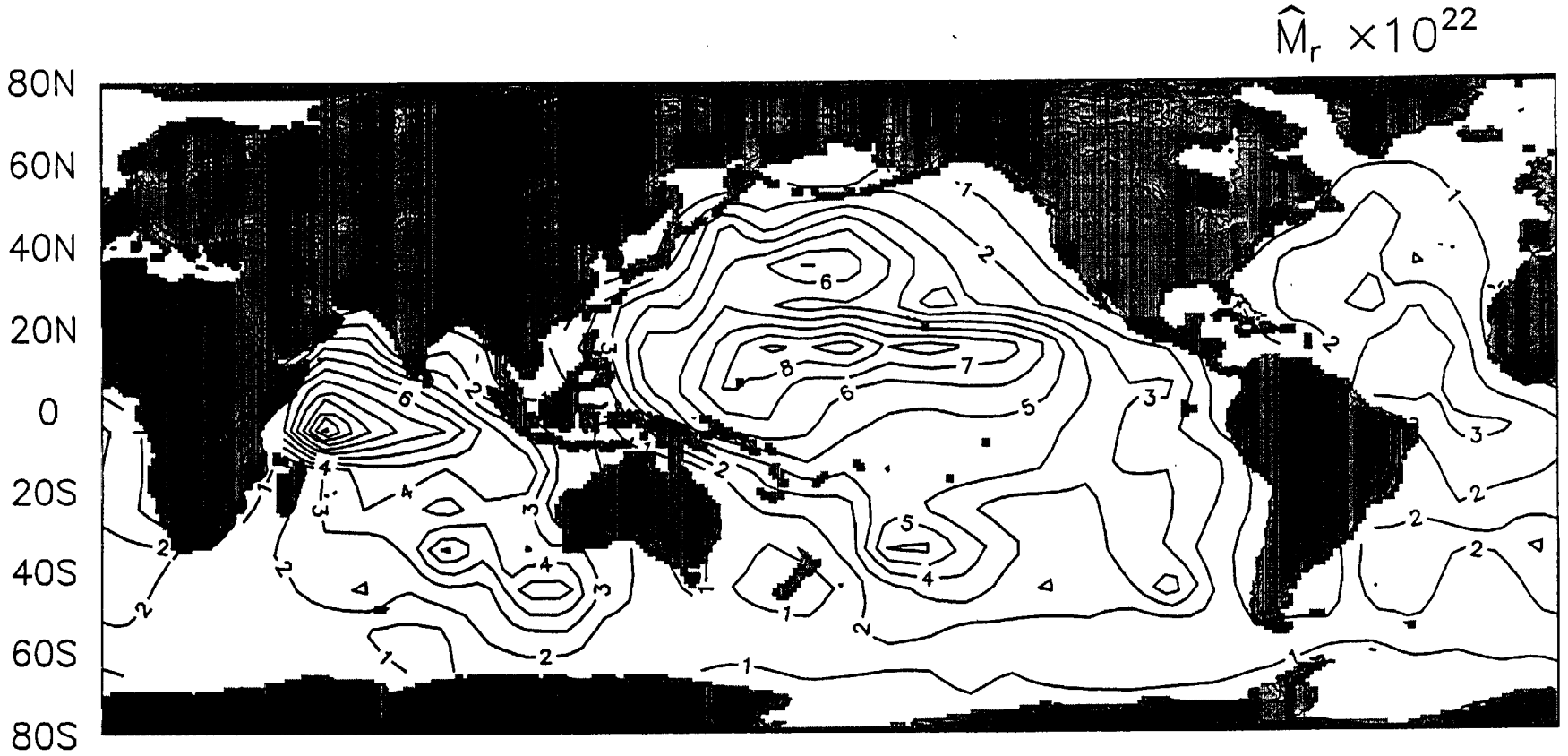
$\hat{M}_r \times 10^{22}$
80N
60N
40N
20N
0
20S
40S
60S
80S
CONTOUR FROM 1 TO 12 BY 1

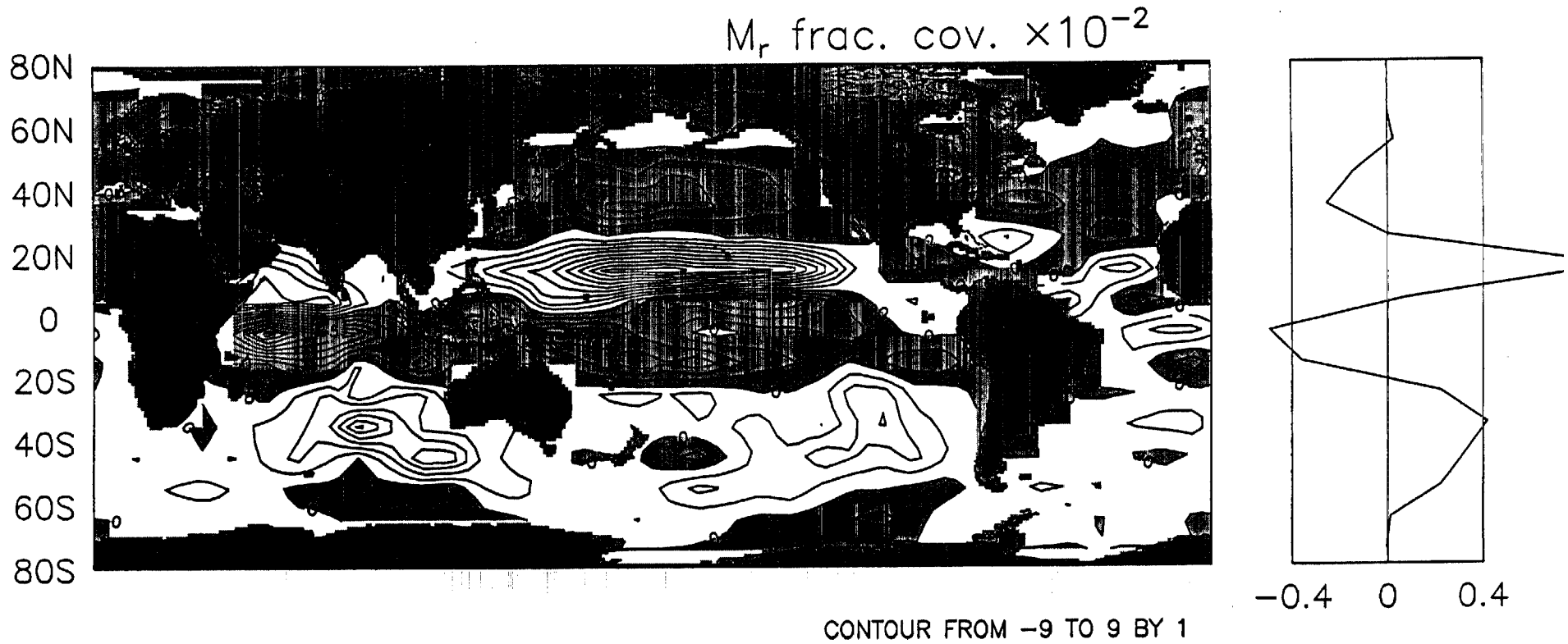
M_r frac. cov. $\times 10^{-2}$
80N
60N
40N
20N
0
20S
40S
60S
80S
−0.4
0
0.4
CONTOUR FROM −9 TO 9 BY 1

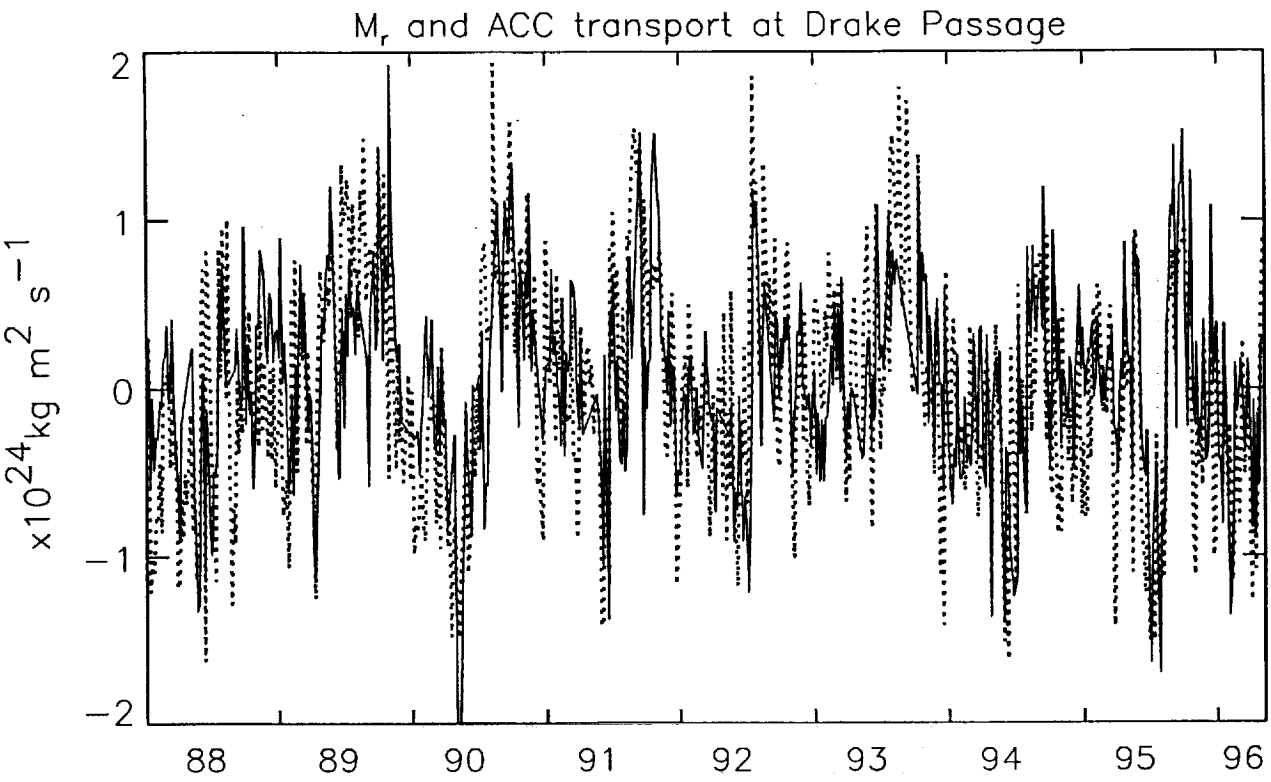
M$_r$ and ACC transport at Drake Passage
x10^{24}kg m^2 s^{-1}
2
1
0
−1
−2
88
89
90
91
92
93
94
95
96

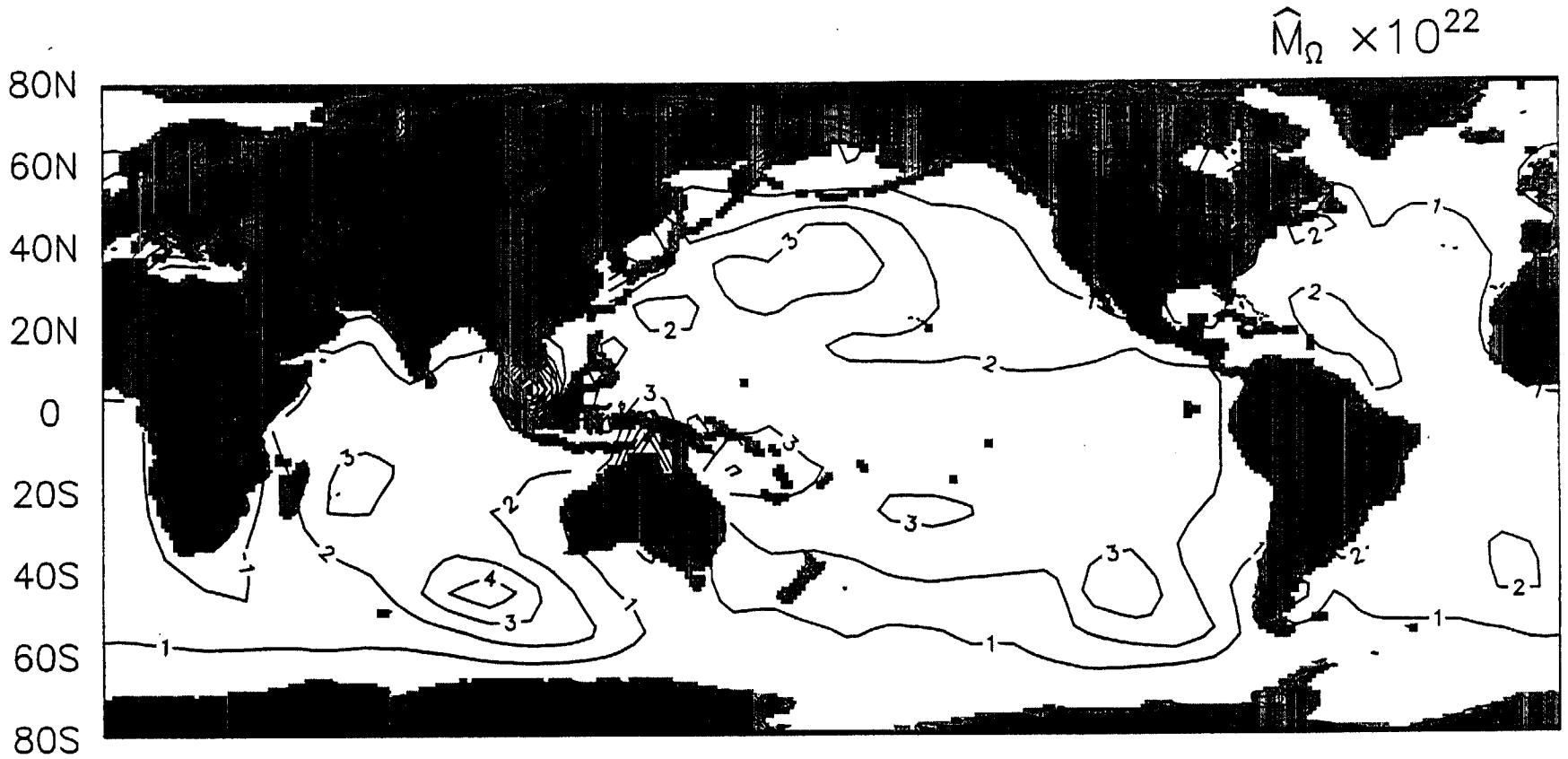
$\hat{M}_\Omega \times 10^{22}$
80N
60N
40N
20N
0
20S
40S
60S
80S
CONTOUR FROM 1 TO 16 BY 1

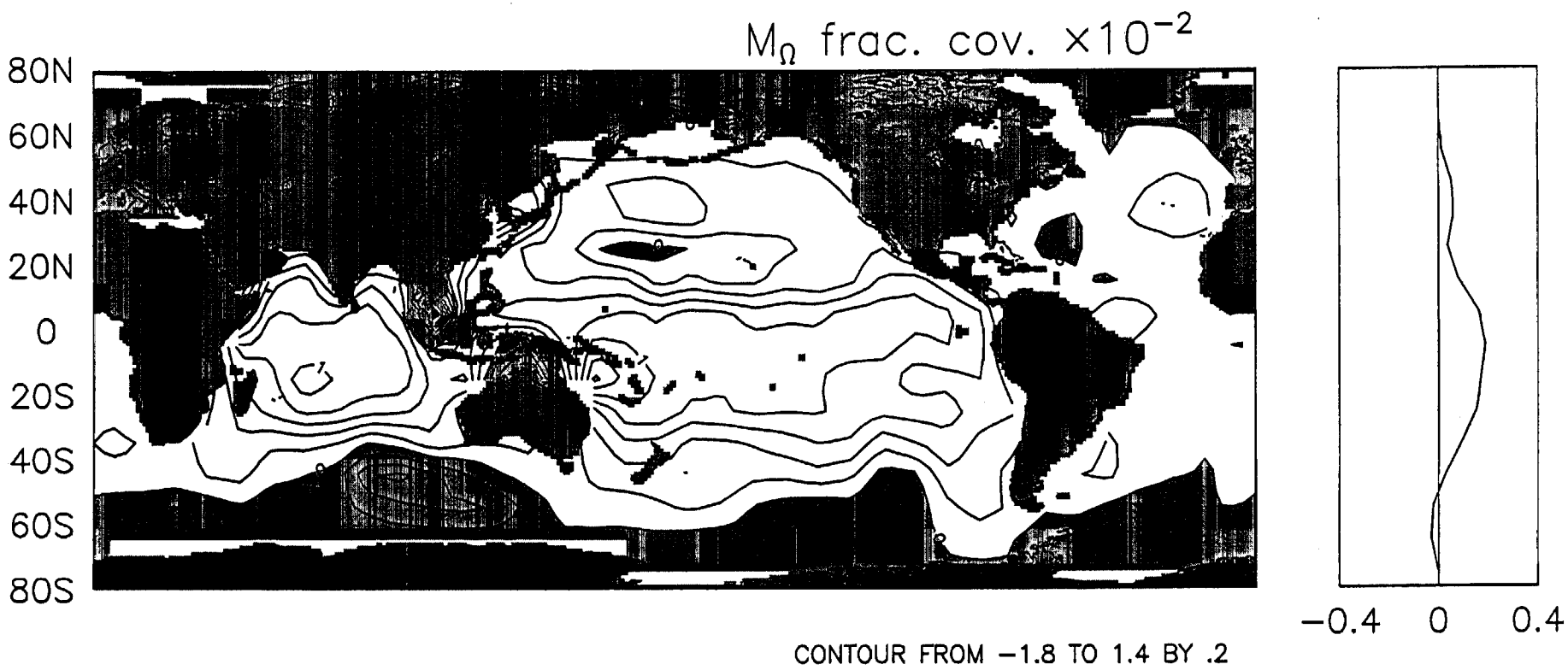

CONTOUR FROM −1.8 TO 1.4 BY .2

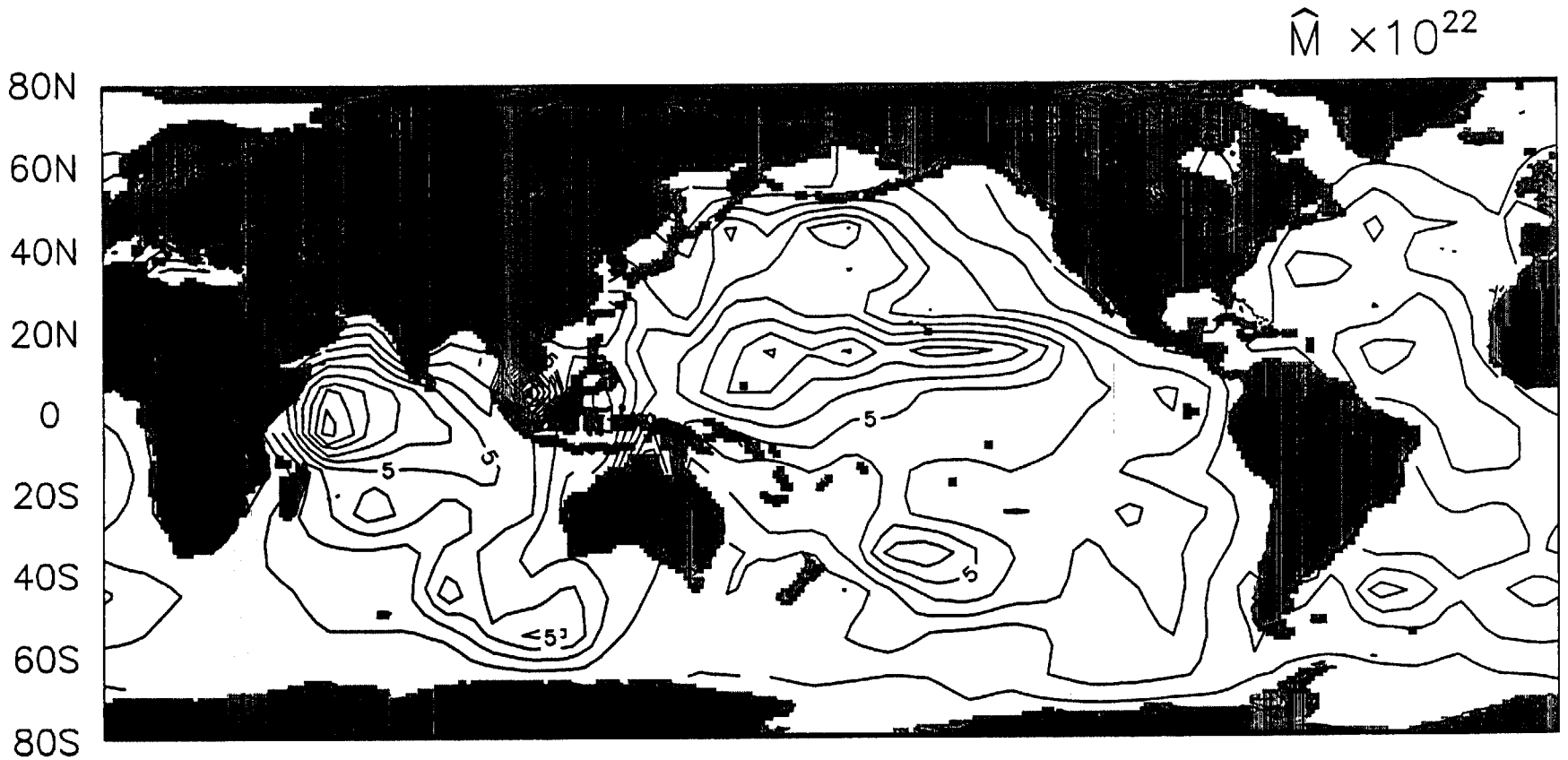

CONTOUR FROM 1 TO 16 BY 1

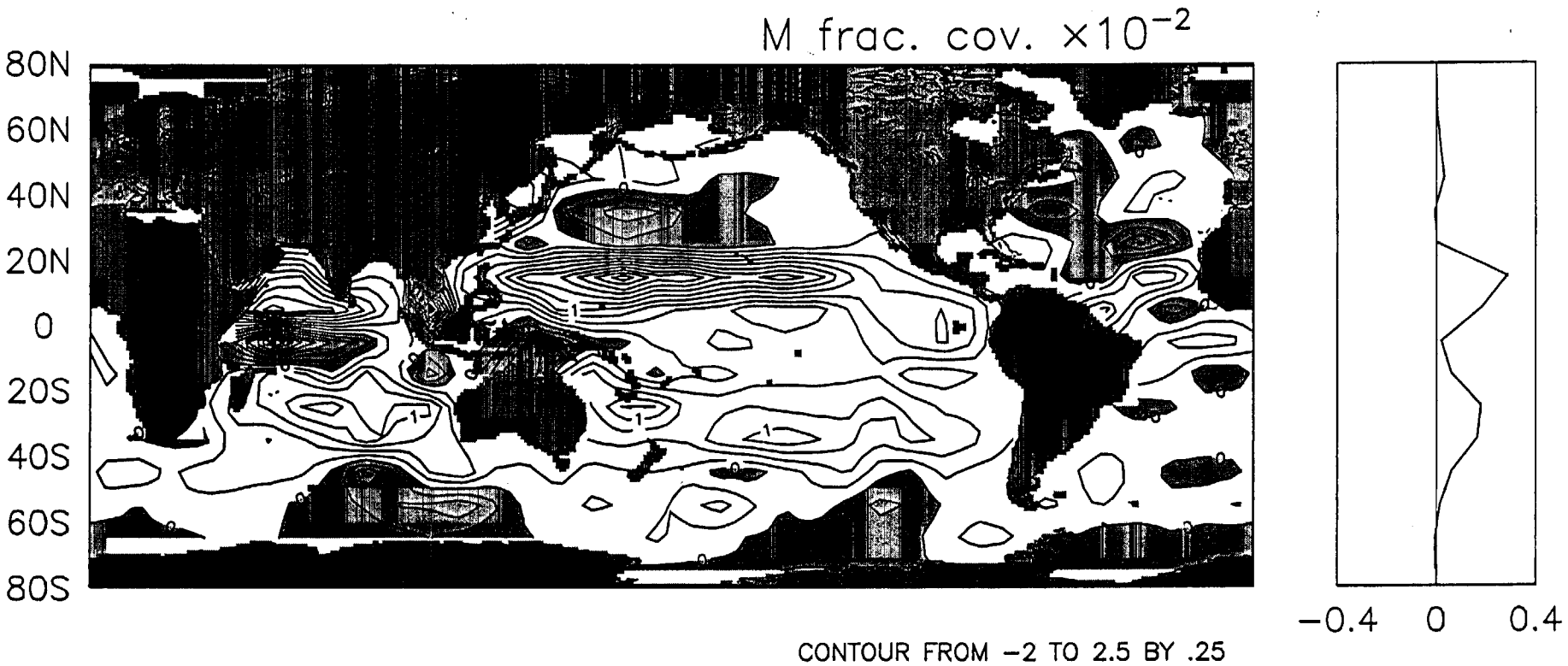
M frac. cov. ×10⁻²
80N
60N
40N
20N
0
20S
40S
60S
80S
−0.4
0
0.4
CONTOUR FROM −2 TO 2.5 BY .25

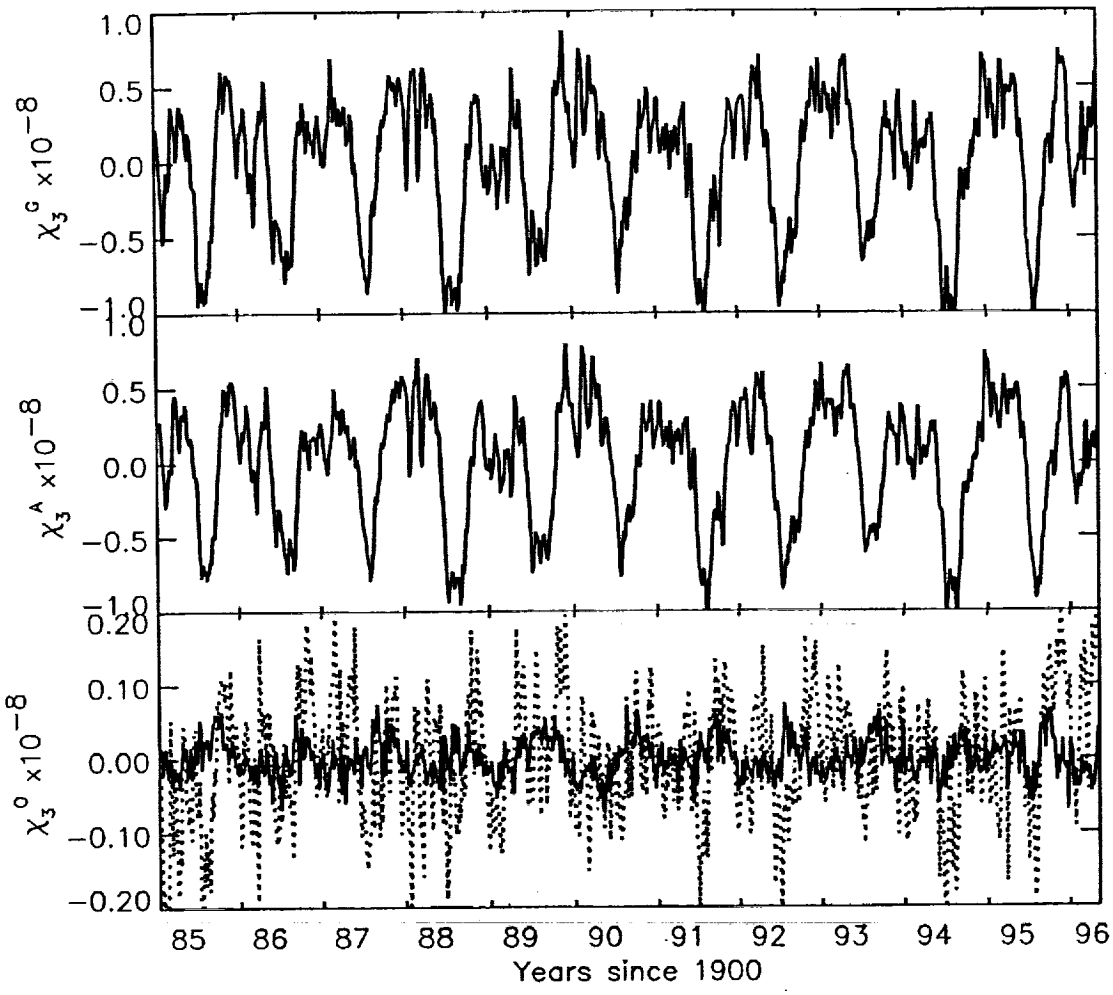
1.0
0.5
0.0
−0.5
−1.0
$\chi_3^G \times 10^{-8}$
1.0
0.5
0.0
−0.5
−1.0
$\chi_3^A \times 10^{-8}$
0.20
0.10
0.00
−0.10
−0.20
$\chi_3^o \times 10^{-8}$
85
86
87
88
89
90
91
92
93
94
95
96
Years since 1900

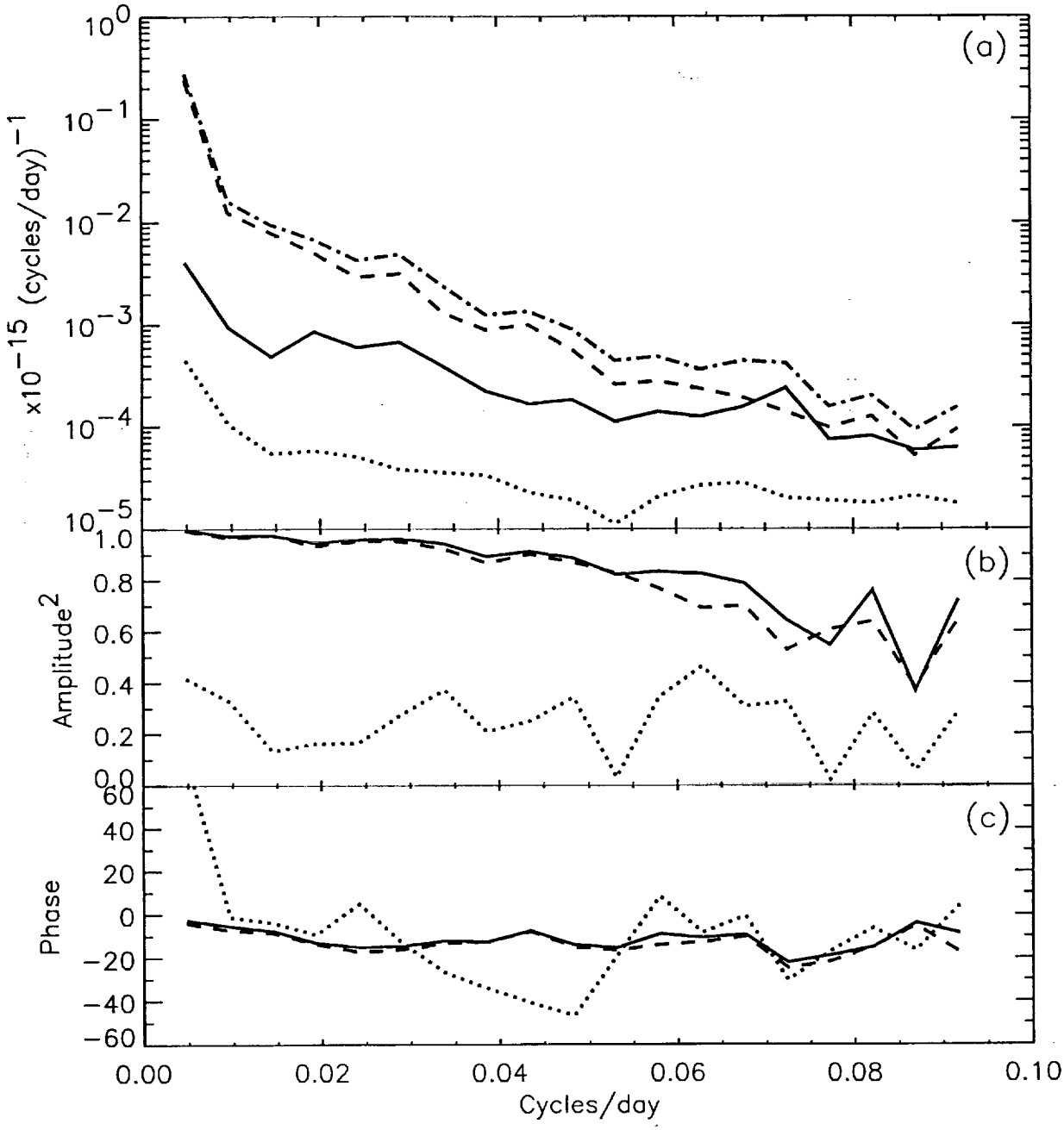
(a)
(b)
(c)
10^0
10^{-1}
10^{-2}
10^{-3}
10^{-4}
10^{-5}
x10^{-15} (cycles/day)$^{-1}$
Amplitude^2
1.0
0.8
0.6
0.4
0.2
0.0
Phase
60
40
20
0
−20
−40
−60
0.00
0.02
0.04
0.06
0.08
0.10
Cycles/day